Journal of Computational Chemistry

WILEY

Journal of COMPUTATIONAL CHEMISTRY

RESEARCH ARTICLE OPEN ACCESS

Computational Insights Into Corrosion Inhibition Mechanism: Dissociation of Imidazole on Iron Surface

Weina Zhao[1,2] | Chang Shen[1] | Anil Kumar Tummanapelli[2] | Ming Wah Wong[2]

[1]Guangdong Key Laboratory of Environmental Catalysis and Health Risk Control, Guangdong-Hong Kong-Macao Joint Laboratory for Contaminants Exposure and Health, Institute of Environmental Health and Pollution Control, School of Environmental Science and Engineering, Guangdong University of Technology, Guangzhou, China | [2]Department of Chemistry, National University of Singapore, Singapore

Correspondence: Weina Zhao (zhaowngd@gdut.edu.cn) | Ming Wah Wong (chmwmw@nus.edu.sg)

Received: 30 September 2024 | **Revised:** 6 January 2025 | **Accepted:** 9 January 2025

Funding: This work was supported by National Natural Science Foundation of China, 22006023; National University of Singapore, R-143-000-B05-114; Guangdong Provincial Key R&D Program, 2022-GDUT-A0007; Natural Science Foundation of Guangdong Province, 2019A1515010428.

Keywords: corrosion inhibition | DFT calculations | dissociation mechanism | imidazole

ABSTRACT

Corrosion inhibitors are widely used to mitigate safety risks and economic losses in engineering, yet post-adsorption processes remain underexplored. In this study, we employed density functional theory calculations with a periodic model to investigate the dissociation mechanisms of imidazole on the Fe(100) surface. Imidazole was found to adsorb optimally in a parallel orientation, with an adsorption energy of −0.88 eV. We explored two dissociation pathways: C—H and N—H bond cleavages and found C—H dissociation having a lower activation barrier of 0.46 eV. Intriguingly, an alternative indirect route C—H dissociation pathway involving a tilted intermediate state was found to be competitive. Both indirect and direct C—H dissociation pathways are energetically more favorable than N—H cleavage. Molecular dynamics simulations reveal that indirect C—H dissociation occurs rapidly. This study proposes an alternative protective mechanism involving dissociated imidazole inhibitors, offering new insights for corrosion inhibitor design.

1 | Introduction

Corrosion is a widespread and costly issue that affects a wide range of industries such as infrastructure, transportation, energy, and manufacturing. The development of effective corrosion inhibitors is therefore of paramount importance to mitigate the economic and structural damage caused by this electrochemical process. Extensive scientific and engineering research efforts have been dedicated to advancing our understanding of corrosion and developing preventive measures [1, 2]. Among the various strategies for corrosion mitigation, the utilization of corrosion inhibitors emerges as a particularly effective method for protecting metals in industrial environments [3–5]. Organic compounds containing heteroatoms have been proven as particularly effective in this role [6–11]. The inclusion of heteroatoms in organic corrosion inhibitors enhances their interaction with metal surfaces, leading to the formation of protective films and effectively mitigating corrosion, thus making them highly valuable for ensuring metal durability and longevity in various industrial applications.

Among the diverse classes of organic corrosion inhibitors, imidazole and imidazole derivatives have garnered significant attention for their outstanding performance [12, 13]. Imidazole derivatives are effective due to their strong adsorption on metal surfaces, ability to form protective films, electrochemical stability, solubility, chemical stability, functional group versatility, and environmentally friendly nature. Extensive research has highlighted the effectiveness of imidazole derivatives in preventing corrosion across a range of environments particularly for iron and carbon steel [14–26].

Density Functional Theory (DFT) under periodic boundary conditions and Molecular Dynamics (MD) calculations are

powerful computational methods widely used to study the adsorption properties on metal surfaces and mechanisms of corrosion inhibitors [27–29]. DFT, a quantum mechanical modeling approach, allows for the precise calculation of electronic structure, enabling the identification of adsorption sites, interaction energies, and the electronic properties of inhibitors at the molecular level. This method provides deep insights into the chemical bonding and reactivity of imidazole compounds on metal surfaces. On the other hand, MD simulations offer a dynamic perspective of the behavior of inhibitors in various environments over time, helping to understand diffusion, adsorption dynamics, and the formation of protective films on metal surfaces. Together, DFT and MD calculations complement each other, providing a comprehensive understanding of how imidazole and its derivatives function as effective corrosion inhibitors [11, 14, 15, 20, 30–36], aiding in the design and optimization of more effective compounds for industrial applications. It is worth noting that combining DFT calculations with machine learning-driven quantitative structure–property relationship (QSPR) models has emerged as a promising approach for predicting corrosion inhibition properties [27, 28, 37].

While theoretical studies indicate that imidazole compounds can significantly enhance the anti-corrosion properties of iron materials, further research is necessary to identify the most effective interaction modes and the underlying mechanisms of anti-corrosion. In particular, there is a significant research gap in understanding the processes that occur post-adsorption, specifically the dissociative adsorption behavior of inhibitors. This study uses imidazole as a test case to explore the interaction mechanisms beyond simple adsorption of the corrosion inhibitor on the iron surface. We investigate the mechanisms of C—H and N—H bond dissociation in imidazole on Fe(100) surface using first-principles surface slab-based DFT calculations and DFT-based MD simulations. Additionally, we perform a comparative study of C2-haloimidazoles adsorption and dissociation on the Fe(100) surface, building on the work of Al-Saadi, Wong and co-workers [17]. Previous studies have primarily focused on the adsorption behavior of C2-halogenated imidazole and its derivatives on iron surfaces, as well as the dissociation mechanisms of C-halogenated bonds [17, 30]. In this study, we comprehensively investigate the potential competitive reaction pathways for C—H and N—H bond dissociations on the Fe(100) surface, with a particular focus on both the indirect and direct mechanisms of C2-H dissociation. Through this theoretical investigation, we propose an alternative model for corrosion inhibition via the dissociation mechanism, aiming to bridge the existing knowledge gaps and enhance the understanding of inhibitor interactions on iron surfaces.

2 | Computational Methods

All DFT calculations were carried out using the VASP software [38], employing Perdew–Burke–Ernzerhof (PBE) functional [39] at the generalized gradient approximation (GGA) level. We carried out the spin-restricted fashion in this work. The projector-augmented wave PAW technique [40, 41] was used here to describe the electron–ion interaction. An energy cut-off of 400 eV was chosen for the plane-wave representation of the orbitals. First-order Methfessel-Paxton smearing [42] with a width of 0.2 eV was employed to facilitate self-consistent field (SCF) convergence. For geometry optimizations, depending on the lattice length, the Brillouin zone was sampled with a Monkhorst–Pack mesh [43] of $2\times2\times1$ k-points for the Fe(100) surface. Due to the large unit cell $2\times2\times2\,nm^3$ for the molecular species in the gas phase, the corresponding Brillouin zone was sampled only by Γ-point. Convergence criteria were set such that energy changes during self-consistent field iterations were below 10^{-4} eV, and a force threshold of 2×10^{-4} eV/pm was required for each relaxed atom during geometry optimization. Transition state (TS) structures were located using the nudged elastic band (NEB) method, followed by an application of the dimer method [44].

A periodic model featuring a slab of five closed-packed Fe atomic layers was used, and a vacuum region generally exceeding 1.7 nm between the slabs. In all calculations, the top three Fe layers together with the adsorbates were allowed to relax, while the two bottom layers were fixed at bulk-terminated geometry Fe–Fe = 255 pm, to mimic the bulk conditions. As illustrated in Figure 1, the flat terrace of Fe(100) was modeled by a 4×4 unit

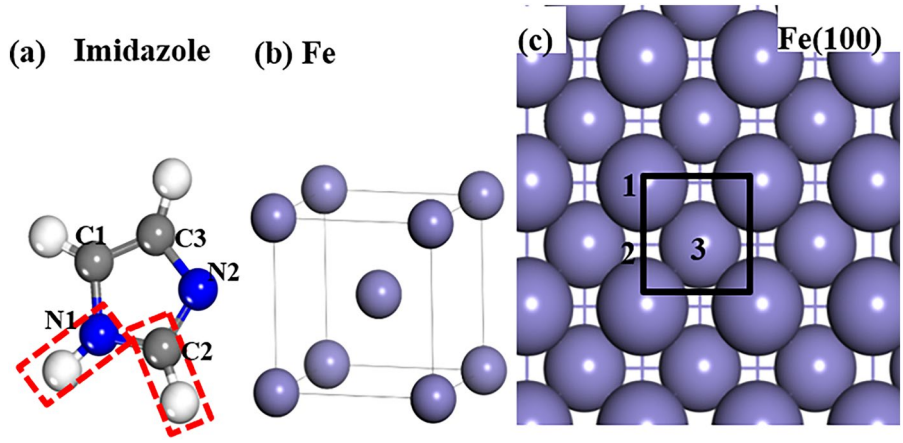

FIGURE 1 | (a) Optimized structures of isolated imidazole, (b) iron bulk and (c) surface models of Fe(100). For clarity, the upper layer of Fe atoms in Fe(100) surface is represented by larger ball size. In the illustrations, Fe is depicted in light blue, C in gray, N in blue, and H in white.

cell. Various adsorption sites for imidazole were considered, including 1 the top site, 2 the bridge site above the midpoint between nearest-neighbor metal atoms, and 3 the hollow site above the center of four neighboring atoms.

The adsorption energy ΔE_{ads} per imidazole (imi) molecule on the surface (sur) is defined by

$$\Delta E_{ads} = E[\text{imi}/\text{sur}] - E[\text{sur}] - E[\text{imi}]$$

where Eimi/sur is the total energy of system, E[sur] is the energy of the pure surface, and E[imi] is the energy of a single imidazole molecule in the gas phase. For each reaction, we also calculate the reaction energy ΔE_r and activation free barrier $\Delta E_a^{\neq}$,

$$\Delta E_r = E[\text{imi} - \text{H}/\text{sur}] - E[\text{imi}/\text{sur}] - E[\text{sur}]$$

$$\Delta E_a^{\neq} = \Delta E(\text{TS}) - \Delta E(\text{imi}/\text{sur})$$

All MD simulations were performed at a temperature of 300 K, with a time step of 0.5 fs. The Nose–Hoover thermostat was used to control the temperature of the NVT ensemble [45]. The initial 500 fs of the simulations served as the equilibration period and was excluded from the data analysis. During the equilibration run, the imidazole molecule was frozen to maintain the TS configuration.

3 | Results and Discussion

3.1 | Adsorbed Species on Fe(100) Surface

To investigate the hydrogen removal mechanism in imidazole, we began by analyzing the key structural characteristics of both adsorbed and dissociated imidazole, that is, co-adsorbed $C_3N_2H_3$ and H on the Fe(100) surface. We first examined the optimized final structures (FS) of the products resulting from C—H dissociation FS_{CH} and N—H dissociation FS_{NH} Figure 2. Following this, we evaluated the general trends in reaction energies and activation barriers to identify the preferred dissociation pathway for imidazole on the Fe(100) surface.

We begin by examining several potential adsorption structures of imidazole on the Fe(100) surface. Three primary adsorption conformations were identified: parallel, perpendicular, and titled structures, with corresponding adsorption energy of −0.88, −0.79, and −0.66 eV. As with in other theoretical studies on adsorption geometries aromatic molecules on metal surfaces [17, 32, 46, 47], the parallel configuration is the most stable adsorption geometry. This parallel conformation IS_{para} and the titled mode IS_{titl}, together with their initial structures (IS), are shown in Figure 2.

It is also insightful to examine the adsorption energies of imidazole on other iron surface facets, specifically Fe(110) and Fe(111). The calculated adsorption energies of the parallel and titled configurations on these two facets are −0.50 and −0.85 eV and −10.5 and −0.97 eV, respectively. In comparison, the Fe(100) facet exhibits moderate surface energy, ranges from −0.6 to −0.8 eV, higher than the stable Fe(110) surface but lower than the reactive

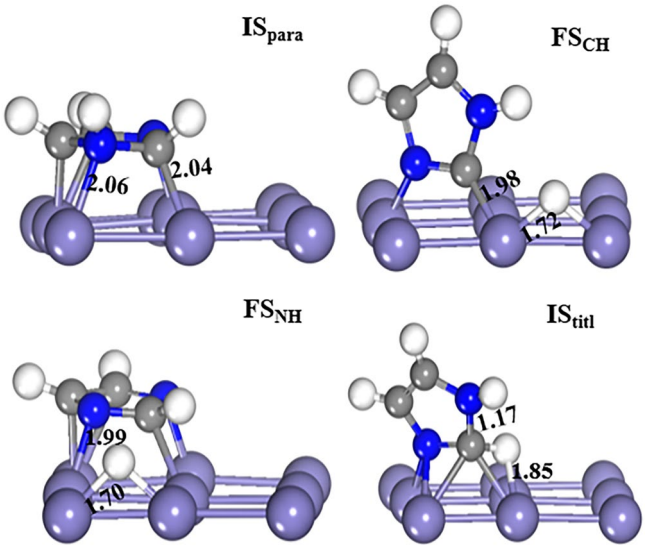

FIGURE 2 | Optimized structures of the most favorable initial state IS_{para} and IS_{titl} and the corresponding dissociated states of C—H FS_{CH} and N—H FS_{NH} cleavage of imidazole on the Fe(100) surface, with key structural parameters given in Å.

Fe(111) surface, making Fe(100) an intermediate case, balancing stability and reactivity. This balance makes it particularly suitable for studying the adsorption behavior of inhibitors and the early stages of corrosion. Furthermore, the Fe(100) surface provides more uniform and accessible active sites for adsorption compared to other facets. Based on these considerations, the Fe(100) surface was selected for further calculations to facilitate a more detailed investigation of imidazole dissociation.

In the IS_{para} configuration, imidazole adsorbs parallelly to the surface with N1, N2, and C2 atoms numbering of the imidazole atoms are given in Figure 1a bonded to the surface Fe atoms, with C—Fe = 2.04 Å and N—Fe = 2.06 Å. Both C1 and C3 atoms are located on the same Fe site, consistent with the previous theoretical finding [30]. In the titled structure in Figure 2, an ~45° angle is observed between the imidazole molecule and the Fe surface. Notably, one of the H atoms approaches the Fe surface, forming a H—Fe bond of 1.85 Å. It is interesting to note that the C2—H bond length in the titled mode (1.17 Å) is significantly longer than that of the parallel configuration (1.09 Å).

Based on the geometries of the dissociated imidazole, that is, co-adsorbed $C_3N_2H_3$ and H in Figure 2, we can determine the reaction energy of imidazole dissociation on Fe(100). For the product of C—H dissociation, the dissociated H atom preferably occupies the bridge site while the $C_3N_2H_3$ species plane is almost perpendicular to the surface. In the case of N—H dissociation, the $C_3N_2H_3$ species also preferentially adsorbs at a site similar to that of the intact imidazole molecule and the H atom favoring the bridge site. Notably, after either C—H dissociation or N—H dissociation, the $C_3N_2H_3$ species moves close to the surface with significantly shorter C—Fe/N—Fe bond length of 1.98/1.99 Å. This clearly indicates the formation of stronger C/N—Fe chemical bonds compared to those in the adsorbed imidazole.

3.2 | Imidazole Dissociation on Fe(100) Surface

3.2.1 | Direct Dissociation

To gain deeper insights into the mechanism and kinetics of imidazole dissociation, we examined the direct cleavage of C2—H and N1—H bonds on iron surface. The calculated reaction energies E_r/eV and activation barriers are summarized in Table 1. Both direct dissociations of C2—H and N1—H in imidazole are exothermic, with calculated reaction energies of −0.63 and −0.44 eV, respectively, indicating the feasibility of imidazole dissociation on the Fe(100) surface, without considering the entropic contribution. The resulting dissociated structure of co-adsorbed C2 dehydrogenated imidazole is a more stable species on the iron surface than N1 dehydrogenated counterpart.

Furthermore, we examined the TSs for C2—H and N1—H bond cleavages of imidazole on Fe(100) to elucidate the kinetics of imidazole dissociation. The schematic dissociation energy profiles are shown in Figure 3a. The calculated barrier of C2—H bond cleavage is 0.46, 0.30 eV lower than that of N1—H bond breaking. It is important to note that the activation barrier of ~0.5 eV can be readily overcome at room temperature. In the TS_{CH}, the C—H bond breaking distance is 1.79 Å, while the H atom attaches to the nearest surface Fe atom at a distance of 1.61 Å distance. Notably, the N1, C2, and C3 atoms in TS_{CH} move upward from the parallel orientation, leading an angle of ~70° between the imidazole backbone and the Fe surface (Figure 3b). Conversely, in TS_{NH}, the N—H bond breaking distance is 1.53 Å, with the H atom positioned on its nearest surface Fe atom at a distance of 1.70 Å. Unlike TS_{CH}, all five imidazole backbone atoms in TS_{NH} remain parallelly adsorbed to the surface (see Figure 3b).

3.2.2 | Indirect Dissociation via Titled Structure

The direct dissociation calculations indicate that the cleavage of the C2–H bond is more favorable than that of the N1–H bond. It is instructive to consider also whether an alternate route exists that can facilitate the C2—H bond cleavage. We explored an indirect dissociation mechanism, which involves an initial transformation from a parallel to a tilted imidazole adsorption structure, followed by the cleavage of the C–H bond. We did not investigate the indirect dissociation of N–H bond, as it is likely a high-energy process due to the N–H bond being positioned too far from the Fe surface in the tilted adsorbed structure. It is noteworthy that Kokalj and co-workers [48] have demonstrated that on copper surfaces, imidazole can undergo dissociative adsorption through cleavage of either the C—H bond in an upright adsorbed geometry or the N—H bond in a lying down adsorbed geometry.

As evidenced in Table 1 and Figure 4a, the transformation from parallel to tilted imidazole is a slightly endothermic process 0.16 eV. However, the predicted activation barrier of 0.40 eV can be easily surmounted at room temperature. In the optimized TS1 geometry (see Figure 4b), the imidazole backbone lifts from the parallel mode, causing the bond breaking of N1,

TABLE 1 | Calculated reaction energies E_r/eV and activation barriers E_a/eV for the C—H and N—H dissociation of imidazole on Fe(100), together with the key parameters of $d_{H\text{-}C/N}$ Å in TS between H atom of imidazole and its nearest Fe atom trapping the hydrogen on the surface.

Reaction	E_r	E_a	$d_{H\text{-}C/N}$
Direct			
C2—H	−0.63	0.46	1.79
N1—H	−0.44	0.76	1.53
Indirect			
Trans[a]	0.16	0.40	—
C2—H	−0.71	0.01	1.21

[a]Transformation from the parallel to tilted adsorption structure.

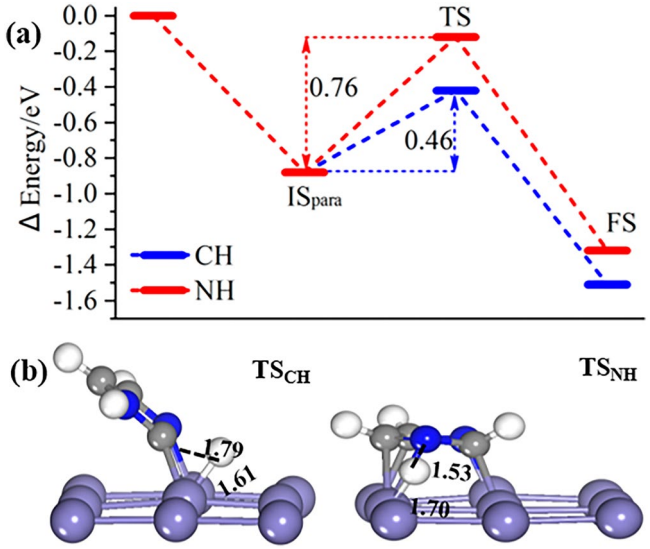

FIGURE 3 | (a) Schematic energy profiles for C—H and N—H directly dissociation in imidazole on Fe(100) surface. (b) Optimized TS geometries of C—H TS_{CH} and N—H TS_{NH} dissociations.

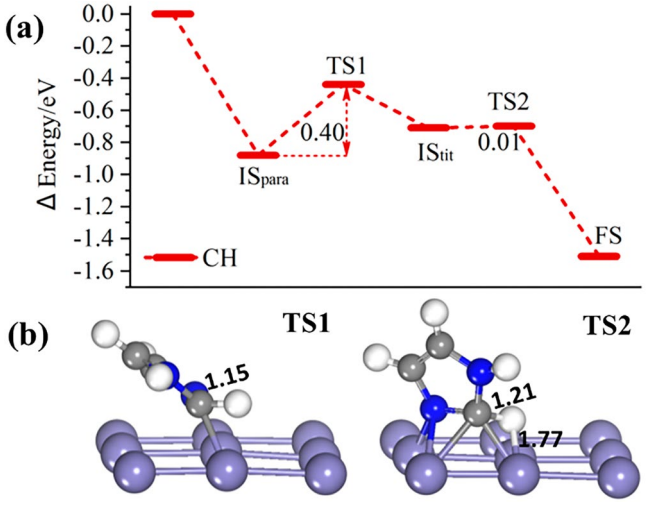

FIGURE 4 | (a) Energy profiles for indirect C-H dissociation in imidazole via the titled intermediate on Fe(100) surface; (b) Calculated TS1 for transformation from parallel to tilted structure, and TS2 for C—H cleavage in the titled imidazole on Fe(100).

C1, and C3 atoms with the Fe surface. Importantly, both N2 and C2 atoms are still bonded with the Fe surface, resembling the tilted adsorption mode. Notably, there is no dissociation of the C1—H bond at this step, with the bond length remaining at 1.15 Å. In the subsequent step involving C2—H bond cleavage, the tilted configuration is highly susceptible to dissociation. The calculated activate barrier is very low ~0.01 eV and the reaction is exothermic by 0.71 eV, consistent with previous study on copper surface [48]. As shown in Figure 4b, the calculated C—H bond distance in TS2 is 1.21 Å, slightly longer than that of the adsorbed imidazole/Fe(100) system 1.17 Å, whereas a shorter value of 1.09 A is in the isolated imidazole molecule. This clearly indicates that the C2–H bond dissociation in the titled mode is imminent.

In summary, our computational results indicate that the C2–H dissociation of imidazole is significantly favored over N–H dissociation on Fe(100) surface Figure 3a. The overall dissociation energetics is summarized as follows: (i) The adsorption of imidazole on Fe(100) IS_{para} is exothermic, with an adsorption energy of −0.88 eV. (ii) The calculated activation barriers of C2—H and N—H cleavages are 0.46 and 0.76 eV, respectively. (iii) The final state of co-adsorbed C2-dehydrogenated imidazole is more stable than that of the N1-dehydrogenated product. (iv) The indirect C2—H fragmentation of imidazole through the titled intermediate offers a more competitive pathway than the direct dissociation, aligning with the findings of a previous DFT study by Kokalj [30].

3.2.3 | Molecular Dynamics Simulations

As demonstrated in our NEB studies, the dissociation of the C2—H bond is more favorable than that of the N1—H bond. To further explore the favorable C—H dissociation reaction, MD simulations were conducted. Since ab initio MD simulations starting from the most stable parallel structure and conducting them for C2—H bond dissociation is a computationally demanding process. To circumvent this challenge, the MD simulations were carried out by considering the titled imidazole mode on Fe(100) as the starting point.

Figure 5 depicts the time evolution of the C2—H bond dissociation of imidazole during the MD simulation. The C2—H dissociation was observed to occur within 2 ps. We also examined snapshots taken at various time intervals along the trajectory. Notably, the C2—H bond breaks on Fe(100) surface in a short time of 920 fs, followed by the separation of dissociated hydrogen from imidazole, which occurs after 1.5 ps. The MD results here align with previous study on C2-halogenated imidazoles [17], confirming that the tilted conformation is kinetically unstable, leading to easy cleavage of the C—H bond. It is worth noting that Kokalj hypothesized that this layer of dissociated products is the key factor responsible for the corrosion inhibition properties of imidazole [30].

What is the physical origin of the favorable C—H dissociation in imidazole? To further understand the dissociation mechanism of the tilted configuration of imidazole adsorbed on the Fe(100) surface, projected density of states PDOS was calculated as shown in Figure 6. The DOS curves of the Fe_{15} atom,

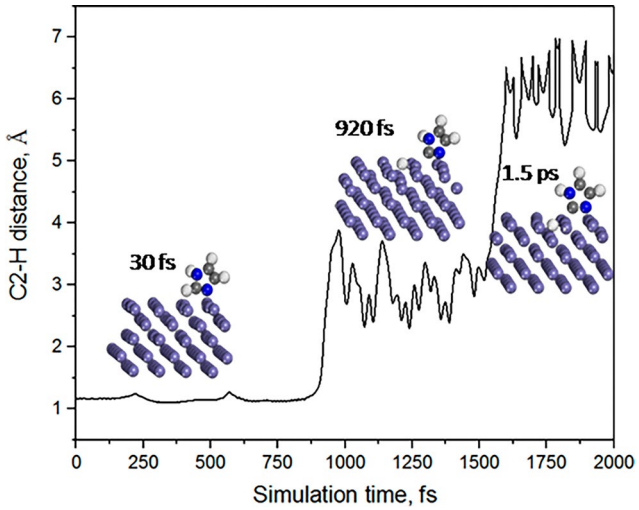

FIGURE 5 | The time evolution of C2—H bond distance during the MD simulations. Snapshots depict various conformations sampled throughout the trajectory.

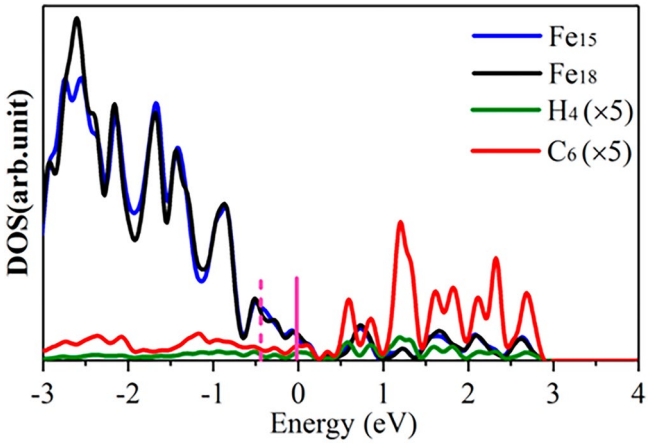

FIGURE 6 | The projected density of states PDOSs for the C_6 and H_4 atom of the imidazole, surface Fe_{15} and Fe_{18} atoms. C_6: Which is bounded to the surface; H_4: Which is bound with C_6 atom; Fe_{15}: The surface Fe atoms in the left row bonded with imidazole; Fe_{18}: The surface Fe atoms in the right row bonded with imidazole.

which is bound to imidazole on the left side of Fe(100) surface, and the Fe_{18} atom, which is bound to imidazole on the right side, are very similar. The DOS peak at the valence band closest to the Fermi level is situated approximately at −0.5 eV. The high degree of electron hybridization indicates a strong bonding interaction between the surface Fe atoms and the adsorbed imidazole.

For the C—H bond adsorbed on the surface of Fe(100), C6 atom displays significantly higher activity compared to H4 atom, showing a greater degree of electron hybridization with surface Fe atoms than that of H atom. This observation indicates that the C atoms readily form bonds with Fe atoms, rendering C—H dissociation more prone to occur. This is further supported by the weaker C2—H bond length (1.17 Å) of the titled configuration compared to the parallel structure (1.09 Å), which support the enhanced activity and dissociative propensity of this bond. This finding aligns with computational results obtained from energy

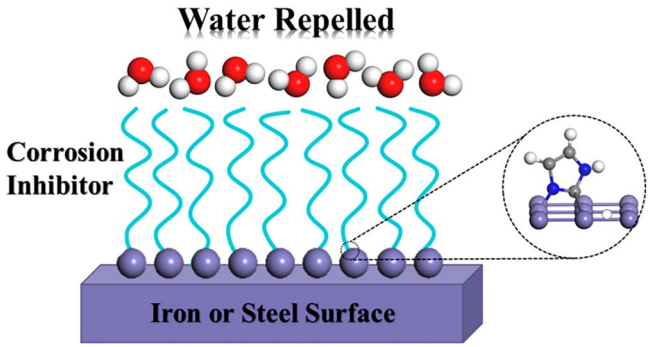

SCHEME 1 | Schematic illustration of dissociated imidazoles as corrosion inhibitors.

profiles and MD simulations, elucidates the relative ease of bond dissociation compared to the parallel structure.

3.2.4 | Alternate Model for Corrosion Inhibition

We believe our theoretical findings here not only elucidate the microscopic mechanism of imidazole as a corrosion inhibitor but also provide an alternative model for corrosion inhibition through molecular dissociation Scheme 1. In this model, when imidazole molecules adsorb onto the iron surface, C—H dissociations occur readily, leading to strongly bounded dehydrogenated species that remain on the surface. These dissociated products are predicted to create a robust protective film over the iron, effectively blocking corrosive agents from penetrating the metal surface. A similar corrosion model was proposed in a combined theoretical and experimental study of the adsorption behavior and corrosion inhibition mechanism of 2-halo-1H-imidazoles [17]. The authors concluded that the tilted conformation of C2-haloimidazole is kinetically unstable, leading to rapid C-halogen bond fragmentation, lead to a tightly adsorbed layer on the iron surface due to halogen-metal interactions. This insight is essential for advancing the screening, design, and development of the next-generation corrosion inhibitors. By understanding the dissociation-based inhibition mechanism, we can better predict the performance of potential inhibitors and tailor molecular structures to enhance their protective capabilities. This model not only provides a deeper understanding of imidazole's inhibitory properties but also offers a framework for exploring other compounds that may operate through similar dissociation-driven mechanisms.

4 | Conclusion

In this study, we utilized state-of-the-art first-principles surface slab calculations and DFT-based MD simulations to investigate the adsorption of imidazole on the clean Fe(100) surface and the dissociation pathways of the adsorbed molecules at a molecular level. We identified three main adsorption conformations: parallel, perpendicular, and tilted, with the parallel structure being the most stable $E_{ad} = -0.88$ eV. The geometries of the imidazole dissociation products indicate stronger C–Fe and N–Fe chemical bonds compared to the corresponding adsorbed imidazole. We considered two possible pathways for the dissociation of imidazole on the Fe(100) surface: direct and indirect dissociation. Previous research has primarily explored on the adsorption behavior of C2-halogenated imidazoles on iron surfaces, the dissociation mechanisms of C-halogenated bonds, and the adsorption behaviors of various organic compounds [17, 30]. In contrast, our study reveals the dissociation mechanisms of C—H and N—H bonds on the Fe(100) surface, emphasizing that the indirect C2—H dissociation pathway, via a titled intermediate state, is energetically more favorable. For direct dissociation, the reaction energies for C—H and N—H cleavages are −0.63 and −0.44 eV, respectively, indicating an exothermic process. The calculated C—H bond dissociation barrier is 0.46 eV, which is 0.3 eV lower than that for the N—H bond rupture on the Fe(100) surface, showing that the C2—H bond is easier to dissociate than the N1—H bond. Additionally, we examined an indirect pathway for imidazole C—H bond dissociation, involving a transformation from a parallel structure to a tilted imidazole adsorption structure, followed by C—H cleavage. Our computational results indicate that the transformation from parallel to tilted imidazole can readily occur at room temperature, making the C2—H bond dissociation likely under the tilted structure. MD simulations further confirmed the favorable indirect process via the tilted intermediate in a short time. In summary, C2—H dissociation is more favorable than N1—H cleavage on Fe(100), and the co-adsorbed C2 dehydroimidazole structure is more stable. Based on the calculated dissociation energetics, we proposed an alternative protective mechanism involving dissociated imidazole inhibitors.

Acknowledgments

This work was supported by the National Natural Science Foundation of China 22006023, the National University of Singapore Grant No: R-143-000-B05-114, Guangdong Provincial Key R&D Program 2022-GDUT-A0007, and the Natural Science Foundation of Guangdong Province 2019A1515010428.

Conflicts of Interest

The authors declare no conflicts of interest.

Data Availability Statement

The data that support the findings of this study are available from the corresponding author upon reasonable request.

References

1. K. Bijapur, V. Molahalli, A. Shetty, A. Toghan, P. D. Padova, and G. Hegde, "Recent Trends and Progress in Corrosion Inhibitors and Electrochemical Evaluation," *Applied Sciences* 13 (2023): 10107.

2. S. Sharma and A. Kumar, "Recent Advances in Metallic Corrosion Inhibition: A Review," *Journal of Molecular Liquids* 322 (2021): 114862.

3. W. Zhao, F. Li, X. Lv, et al., "Research Progress of Organic Corrosion Inhibitors in Metal Corrosion Protection," *Crystals* 13 (2023): 1329.

4. S. Harsimran, K. Santosh, and K. Rakesh, "Overview of Corrosion and Its Control: A Critical Review," *Proceedings on Engineering Sciences* 3 (2021): 13–24.

5. V. S. Sastri, *In Corrosion Inhibitors. Principles and Applications* (Chichester: Wiley, 1998).

6. J. Wang, L. An, J. Wang, J. Gu, J. Sun, and X. Wang, "Frontiers and Advances in N-heterocycle Compounds as Corrosion Inhibitors in Acid Medium: Recent Advances," *Advances in Colloid and Interface Science* 321 (2023): 103031.

7. L. K. M. O. Goni, M. J. A. Mazumder, M. A. Quraishi, and M. M. Rahman, "Bioinspired Heterocyclic Compounds as Corrosion Inhibitors: A Comprehensive Review," *Chemistry–An Asian Journal* 16 (2021): 1324–1364.

8. M. A. Quraishi, D. S. Chauhan, and V. S. Saji, "Heterocyclic Biomolecules as Green Corrosion Inhibitors," *Journal of Molecular Liquids* 341 (2021): 117265.

9. L. Guo, I. B. Obot, X. Zheng, et al., "Theoretical Insight into an Empirical Rule About Organic Corrosion Inhibitors Containing Nitrogen, Oxygen, and Sulfur Atoms," *Applied Surface Science* 406 (2017): 301–306.

10. Y. G. Avdeev, "Nitrogen-Containing Six-Membered Heterocyclic Compounds as Corrosion Inhibitors for Metals in Solutions of Mineral Acids – A Review," *International Journal of Corrosion and Scale Inhibition* 7 (2018): 460–497.

11. M. Ouakki, M. Galai, M. Rbaa, et al., "Investigation of Imidazole Derivatives as Corrosion Inhibitors for Mild Steel in Sulfuric Acidic Environment: Experimental and Theoretical Studies," *Ionics* 26 (2020): 5251–5272.

12. M. Ouakki, M. Galai, and M. Cherkaoui, "Imidazole Derivatives as Efficient and Potential Class of Corrosion Inhibitors for Metals and Alloys in Aqueous Electrolytes: A Review," *Journal of Molecular Liquids* 345 (2022): 117815.

13. A. Mishra, J. Aslam, C. Verma, M. A. Quraishi, and E. E. Ebenso, "Imidazoles as Highly Effective Heterocyclic Corrosion Inhibitors for Metals and Alloys in Aqueous Electrolytes: A Review," *Journal of the Taiwan Institute of Chemical Engineers* 114 (2020): 341–358.

14. A. Barrahi, M. E. Faydy, L. Adlani, et al., "Anticorrosive Characteristics of Imidazole Derivative on Carbon Steel in 1 M HCl," *Journal of Electrochemical Science and Engineering* 14 (2024): 193–212.

15. M. O. Rosales, A. E. Vázquez, F. J. R. Gómez, et al., "Imidazolate of 1-Butyl-3-Ethyl Imidazole as Corrosion Inhibitor on API 5L X52 Steel in NaCl Saturated with CO2," *Journal of Molecular Liquids* 363 (2022): 119826.

16. D. Legut, A. P. Kadzielawa, P. Panek, et al., "Inhibition of Steel Corrosion with Imidazolium-Based Compounds–Experimental and Theoretical Study," *Corrosion Science* 191 (2021): 109716.

17. I. Abdulazeez, A. Zeino, C. W. Kee, et al., "Mechanistic Studies of the Influence of Halogen Substituents on the Corrosion Inhibitive Efficiency of Selected Imidazole Molecules: A Synergistic Computational and Experimental Approach," *Applied Surface Science* 471 (2019): 494–505.

18. B. Dey, S. Suklabaidya, S. Majumdar, P. K. Paul, D. Bhattacharjee, and S. A. Hussain, "Effect of Functional Group on Electrical Switching Behaviour of an Imidazole Derivative in Langmuir-Blodgett Film," *ChemistrySelect* 4 (2019): 9065–9073.

19. M. Ouakki, M. Galai, M. Rbaa, et al., "Quantum Chemical And Experimental Evaluation of the Inhibitory Action of Two Imidazole Derivatives on Mild Steel Corrosion in Sulphuric Acid Medium," *Heliyon* 5 (2019): e02759.

20. A. Duttaa, S. K. Sahab, U. Adhikaria, P. Banerjeeb, and D. Sukula, "Effect of Substitution on Corrosion Inhibition Properties of 2-(Substituted Phenyl) Benzimidazole Derivatives on Mild Steel in 1 M HCl Solution: A Combined Experimental and Theoretical Approach," *Corrosion Science* 123 (2017): 256–266.

21. A. Singh, K. R. Ansari, A. Kumar, W. Liu, S. Chen, and Y. Lin, "Electrochemical, Surface and Quantum Chemical Studies of Novel Imidazole Derivatives as Corrosion Inhibitors for J55 Steel in Sweet Corrosive Environment," *Journal of Alloys and Compounds* 712 (2017): 121–133.

22. E. Gutierrez, J. A. Rodríguez, J. Cruz-Borbolla, J. G. Alvarado-Rodríguez, and P. Thangarasu, "Development of a Predictive Model for Corrosion Inhibition of Carbon Steel by Imidazole and Benzimidazole Derivatives," *Corrosion Science* 108 (2016): 23–35.

23. D. Zhang, Y. Tang, S. Qi, D. Dong, H. Cang, and G. Lu, "The Inhibition Performance of Long-Chain Alkyl-Substituted Benzimidazole Derivatives for Corrosion of Mild Steel in HCl," *Corrosion Science* 102 (2016): 517–522.

24. G. Bhargava, T. A. Ramanarayanan, and S. L. Bernasek, "Imidazole–Fe Interaction in an Aqueous Chloride Medium: Effect of Cathodic Reduction of the Native Oxide," *Langmuir* 26 (2010): 215–219.

25. Z. Zhang, S. Chen, Y. Li, S. Li, and L. Wang, "A Study of the inhibition of Iron Corrosion by Imidazole and its Derivatives Self-Assembled Films," *Corrosion Science* 51 (2009): 291–300.

26. K. F. Khaled, "The Inhibition of Benzimidazole Derivatives on Corrosion of Iron in 1 M HCl Solutions," *Electrochimica Acta* 48 (2003): 2493–2503.

27. S. Li, C. Li, and F. Wang, "Computational Experiments of Metal Corrosion Studies: A Review," *Materials Today Chemistry* 37 (2024): 101986.

28. E. E. Ebenso, C. Verma, L. O. Olasunkanmi, et al., "Molecular Modelling of Compounds Used for Corrosion Inhibition Studies: A Review," *Physical Chemistry Chemical Physics* 23 (2021): 19987–20027.

29. P. Liu, Q. Xu, Q. Zhang, et al., "A New Insight into Corrosion Inhibition Mechanism of the Corrosion Inhibitors: Review on DFT and MD Simulation," *Journal of Adhesion Science and Technology* 38 (2024): 1563-1584.

30. A. Kokalj, "Formation and Structure of Inhibitive Molecular Film of Imidazole on Iron Surface," *Corrosion Science* 68 (2013): 195–203.

31. A. Kokalj, "Comments On The Paper "On the Nature of Inhibition Performance of Imidazole on Iron Surface" by J.O. Mendes, E.C. da Silva, A.B. Rocha," *Corrosion Science* 68 (2013): 286–289.

32. J. O. Mendes, E. C. Da Silva, and A. B. Rocha, "Reply To Comments On The Paper "On the Nature of Inhibition Performance of Imidazole on Iron Surface" by J.O. Mendes, E.C. da Silva, A.B. Rocha," *Corrosion Science* 68 (2013): 290–291.

33. J. Radilla, G. E. Negron-Silva, M. Palomar-Pardave, and M. Galvan, "DFT Study of the Adsorption of the Corrosion Inhibitor 2-Mercaptoimidazole onto Fe(100) Surface," *Electochimica Acta* 112 (2013): 577–586.

34. M. Mousavi, M. Mohammadalizadeh, and A. Khosravan, "Theoretical Investigation of Corrosion Inhibition Effect of Imidazole and its Derivatives on Mild Steel Using Cluster Model," *Corrosion Science* 53 (2011): 3086–3091.

35. M.-F. Chen, Y. Chen, Z. J. Lim, and M. W. Wong, "Adsorption of Imidazolium-Based Ionic Liquids on The Fe(100) Surface for Corrosion Inhibition: Physisorption or Chemisorption?," *Journal of Molecular Liquids* 367 (2022): 120489.

36. Z. Cao, Y. Tang, H. Cang, J. Xu, G. Lu, and W. Jing, "Novel Benzimidazole Derivatives as Corrosion Inhibitors of Mild Steel in the Acidic Media. Part II: Theoretical Studies," *Corrosion Science* 83 (2014): 292–298.

37. C. T. Ser, P. Zuvela, and M. W. Wong, "Prediction of Corrosion Inhibition Efficiency of Pyridines and Quinolines on an Iron Surface Using Machine Learning-Powered Quantitative Structure-Property Relationships," *Applied Surface Science* 512 (2020): 145612.

38. G. Kresse and J. Furthmüller, "Efficiency of Ab-Initio Total Energy Calculations for Metals and Semiconductors Using a Plane-Wave Basis Set," *Computational Materials Science* 6 (1996): 15–50.

39. J. P. Perdew, K. Burke, and M. Ernzerhof, "Generalized Gradient Approximation Made Simple," *Physical Review Letters* 77 (1996): 3865–3868.

40. P. E. Blochl, "Projector Augmented-Wave Method," *Physical Review B* 50 (1994): 17953–17979.

41. P. E. Blochl, C. J. Forst, and J. Schimpl, "Projector Augmented Wave Method: Ab Initio Molecular Dynamics with Full Wave Functions," *Bulletin of Materials Science* 26 (2003): 33–41.

42. T. Bjorkman and O. Granas, "Adaptive Smearing for Brillouin Zone Integration," *International Journal of Quantum Chemistry* 111 (2011): 1025–1030.

43. H. J. Monkhorst and J. D. Pack, "Special Points for Brillouin-Zone Integrations," *Physical Review B* 13 (1976): 5188–5192.

44. G. Henkelman and H. Jonsson, "A Dimer Method for Finding Saddle Points on High Dimensional Potential Surfaces Using Only First Derivatives," *Journal of Chemical Physics* 111 (1999): 7010–7022.

45. D. J. Evans and B. L. Holian, "The Nose–Hoover Thermostat," *Journal of Chemical Physics* 83 (1985): 4069–4074.

46. W. Dou, J. Zhu, Q. Liao, H. Zhang, P. He, and S. Bao, "Monolayer Structure of Tetracene on Cu (100) Surface: Parallel Geometry," *Journal of Chemical Physics* 128 (2008): 244706.

47. T. L. M. Pham, T. K. Phung, and H. V. Thang, "DFT Insights Into The Adsorption Mechanism of Five-Membered Aromatic Heterocycles Containing N, O, or S on Fe(110) Surface," *Applied Surface Science* 583 (2022): 152524.

48. A. Kokalj, D. Gustincic, M. Poberznik, and M. Lozinsek, "New Insights into Adsorption Bonding of Imidazole: A Viable C2–H Bond, Cleavage on Copper Surfaces," *Applied Surface Science* 479 (2019): 463–468.